NIRPS: An Adaptive-Optics assisted radial velocity spectrograph to chase exoplanets around M-stars

F. Wildi*[a], N. Blind[a], V. Reshetov[b], O. Hernandez[c,d], L. Genolet[a], U. Conod[a], M. Sordet[a], A. Segovilla[a], J. L. Rasilla[e], D. Brousseau[f], S. Thibault[f], B. Delabre[g], T. Bandy[h], M. Sarajlic[h], A. Cabral[i,j], S. Bovay[a], Ph. Vallée[c,d], F. Bouchy[a], R. Doyon[c,d], E Artigau[c,d], F. Pepe[a], J. Hagelberg[l], C. Melo[k], X. Delfosse[l], P. Figueira[m], N. C. Santos[m,n], , J. I. González Hernández[e], J. R. de Medeiros[p] , R. Rebolo[e], Ch. Broeg[h], W. Benz[h], I Boisse[o], L. Malo[c,d], U. Käufl[g], L. Saddlemyer[b]

[a]Observatoire Astronomique de l'Université de Genève, 51 Ch. des Maillettes, 1290 Versoix, Switzerland
[b]NRC Canada, Herzberg Institute of Astrophysics, 5071 West Saanich Rd, Victoria, BC, V9E 2E7, Canada
[c]Institut de Recherche sur les Exoplanètes (IREx), Université de, Montréal, QC, Canada.
[d]Observatoire Mont-Mégantic, Dpt de Physique, Université de Montréal, C.P. 6128, Montréal, QC, H3C 3J7, Canada
[e]Instituto de Astrofísica de Canarias (IAC), E-38205 La Laguna, Tenerife, Spain
[f]Département de physique, de génie physique et d'optique, Université Laval, Québec, QC, Canada G1V 0A6
[g]European Southern Observatory, Karl-Schwarzschild-Str. 2, 85748, Garching b. München, Germany
[h]Center for Space and Habitability, University of Berne, CH-3012 Bern, Sidlerstrasse 5, Switzerland
[i]Laboratório de Óptica, Laser e Sistemas da Faculdade de Ciências da Universidade de Lisboa, Portugal
[j]Instituto de Astrofísica, Universidade de Lisboa, Estrada do Paço do Lumiar 22, PT1649-038 Lisboa, Portugal
[k]European Southern Observatory, Alonso de Córdova 3107, Vitacura, Casilla 19001, Santiago 19, Chile
[l]Institut de Planétologie et d'Astrophysique de Grenoble, Univ. Grenoble Alpes, CNRS, F-38000 Grenoble, France
[m]Instituto de Astrofísica, Universidade do Porto, CAUP, Rua das Estrelas, 4150-762 Porto, Portugal
[n]Departamento de Física e Astronomia, Universidade do Porto, Rua do Campo Alegre, 4169-007 Porto, Portugal
[o]Aix Marseille Université, CNRS, Laboratoire d'Astrophysique Marseille UMR 7326, 13388 Marseille cedex 13, France
[p]Departamento de Física, Universidade Federal do Rio Grande do Norte, 59072-970 Natal, RN, Brazil

ABSTRACT

Since 1st light in 2002, HARPS has been setting the standard in the exo-planet detection by radial velocity (RV) measurements[1]. Based on this experience, our consortium is developing a high accuracy near-infrared RV spectrograph covering YJH bands to detect and characterize low-mass planets in the habitable zone of M dwarfs. It will allow RV measurements at the 1-m/s level and will look for habitable planets around M- type stars by following up the candidates found by the upcoming space missions TESS, CHEOPS and later PLATO.

NIRPS and HARPS, working simultaneously on the ESO 3.6m are bound to become a single powerful high-resolution, high-fidelity spectrograph covering from 0.4 to 1.8 micron. NIRPS will complement HARPS in validating earth-like planets found around G and K-type stars whose signal is at the same order of magnitude than the stellar noise.

Because at equal resolving power the overall dimensions of a spectrograph vary linearly with the input beam étendue, spectrograph designed for seeing-limited observations are large and expensive. NIRPS will use a high order adaptive optics system to couple the starlight into a fiber corresponding to 0.4" on the sky as efficiently or better than HARPS or ESPRESSO couple the light 0.9" fiber. This allows the spectrograph to be very compact, more thermally stable and less costly. Using a custom tan(θ)=4 dispersion grating in combination with a start-of-the-art Hawaii4RG detector makes NIRPS very efficient with complete coverage of the YJH bands at 110'000 resolution.

NIRPS works in a regime that is in-between the usual multi-mode (MM) where 1000's of modes propagates in the fiber and the single mode well suited for perfect optical systems. This regime called few-modes regime is prone to modal noise- Results from a significant R&D effort made to characterize and circumvent the modal noise show that this contribution to the performance budget shall not preclude the RV performance to be achieved.

Keywords: exoplanets, radial velocity spectrograph, few mode fibers

*francois.wildi@unige.ch

1. NIRPS SCIENCE CASE

High-precision radial velocity (RV) measurements have led to the first confirmation of exoplanet discoveries in the mid-90's, and remained by far the most efficient discovery method until the launch of the Kepler mission. In the era of abundant exoplanet discoveries made by transit searches, RV measurements remain essential on two important fronts. Firstly they provide a mass measurement of transiting planets, whereas the transit itself provides a radius measurement. These combined measurements lead to a determination of planet density and constrain their bulk composition. Secondly, the vast majority of exoplanets do not transit their host star from our point of view, so establishing a complete census of nearby exoplanets cannot be done with the transit method, and is best performed through radial velocity measurements.

While the progress made in exoplanet study over the last two decades is commanding, we have only begun the study of potentially habitable Earth-like planets around nearby stars. While the Earth-likeness of a planet is a somewhat arbitrary concept, it is generally thought of as a terrestrial planet in the zone around its star where it could host liquid water at its surface. While finding an Earth analog around a Sun-like star is still beyond the capacity of current RV spectrographs, M dwarfs offer an appealing short cut to the study of these planets. M dwarfs are lighter than our Sun (7-50%), have smaller radii (0.1-0.5 R_{sol}) and are significantly cooler (2400 to 4000K versus 5700K), all of which conspire to increase the radial-velocity signal of a planet in their habitable zone. An Earth-mass planet with an Earth-like equilibrium temperature around a late-M will lead to an RV signature >10 times larger than that of the Earth, which makes its detection possible with existing technology. NIRPS is designed to detect M-dwarf planets by obtaining RV measurements over the peak of their spectral energy distribution in the near-infrared domain.

RV planet detection is, even with a perfect instrument, limited by our ability to filter-out spurious signals due to the star itself. The presence of stellar activity induces RV signals that can mask planetary signals. M dwarfs are known to be active and many display stellar spots and flares, which need to be accounted for in our analysis. As activity RV signatures are chromatic, contrary to the planet-induced RV motion, the simultaneous observation with NIRPS and HARPS over the 0.4-1.8µm domain will enable the filtering of stellar activity better than would be possible with an instrument operating only in a single domain. This will be particularly important for early-to-mid-M dwarfs, where NIRPS and HARPS are expected to have a similar RV accuracy.

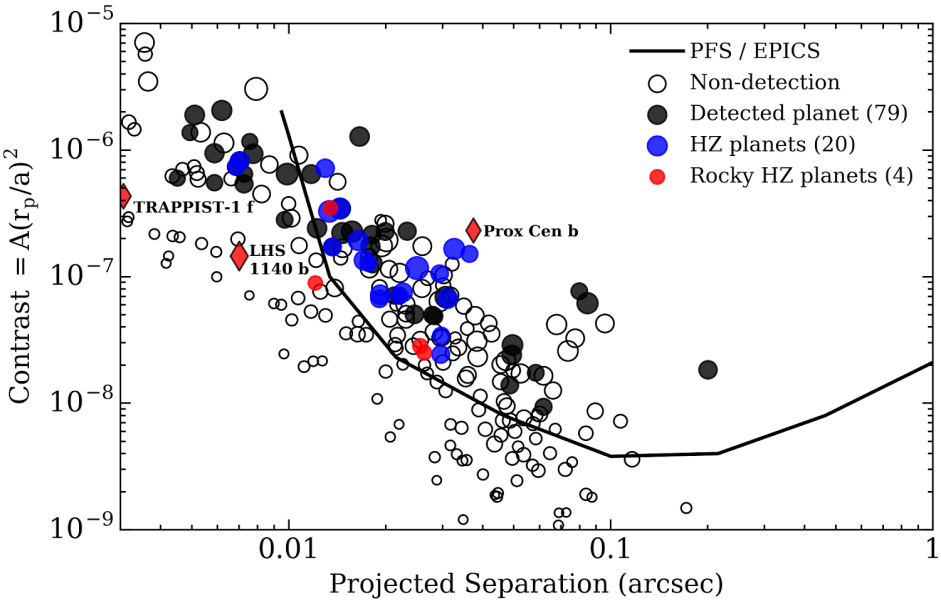

Figure 1 - Simulated NIRPS planet population in the projected separation/contrast plane. A geometrical albedo of A=0.3 is assumed for all planets. Shaded circles represent planets that would be detected with NIRPS; detected HZ planets are highlighted in blue and detected rocky (rp < 1.5 R⊕) HZ planets highlighted in red. The planet population is compared to the expected contrast curve expected to be achieved by third generation of ELT near-IR imagers. Red diamonds show the estimated location of nearby HZ planets around M dwarfs.

Three main surveys will be performed through the Guaranteed Time Observations (700 night over 5 years). Firstly, we will survey M dwarfs in the immediate vicinity of the Sun to identify the nearest terrestrial planets. The proximity of these planets puts them within reach of the high-contrast imagers foreseen as third-generation instruments on the ELTs (e.g., EPICS/PFS). Discovering a sample of planets that can be directly imaged within a timescale of a decade or so would strongly bolster the case for this type of instrument. Figure 1 illustrates a representative predicted sample of exoplanets detected by the NIRPS survey and their detectability for high-contrast imagers.

Secondly, we will perform follow-ups of M dwarf planets uncovered by the upcoming TESS mission, as well as a suite of ground-based experiments (e.g., ExTRA, TRAPPIST, NGTS, Mearth). Establishing the mass of a planet is key in preparing follow-up transit spectroscopy with JWST, and in the physical interpretation of the transit spectrum. Finally, we will dedicate GTO time to the atmospheric characterization of known transiting exoplanets through very high-resolution transit spectroscopy. Space-based transit spectroscopy, such as will be possible with JWST, provide low to intermediate spectral resolution and inform on broad molecular features and the relative strength of various absorbers. NIRPS+HARPS transit spectroscopy will provide complementary information on line profiles in planetary spectra, which in turn informs us on planetary winds and heat transport in these atmospheres.

2. INSTRUMENTAL CONCEPT

To address the science case described above we develop a radial velocity spectrograph based on a very short set of top level technical requirements:

- A spectrograph operating in the Y, J, H bands, optionally include the K band.
- High spectral resolution of about R = 100 000 to best exploit the spectral content
- High-RV precision and high spectral fidelity at a level corresponding to the 1m/s over short and long time scales (years), in order to execute coherent and long-lasting programs.
- Reach a photon noise of 1 m/s in <30min for an M3 with H=9
- Bright limit of H<1.7 as to observe bright, nearby, stars
- Fiber-fed spectrograph. The on-sky diameter of the fiber should be smaller than 1.2”

To which we add a couple of operational requirement

- First light in 2019, full science operation by early-2020
- Designed for the ESO 3.6m telescope in La Silla. Simultaneous operation of HARPS and NIRPS (since HARPS is the workhorse on this telescope.
- Observational efficiency: < 2 minute setup overheads

It is important to understand that the spectrograph itself is NOT the only part paying an important role in the performance of a RV spectrograph and in NIRPS in particular. As matter of fact there are three sub-systems in NIRPS:

1. The *front-end* which extracts the 700nm-2400nm band from the telescope beam, corrects for atmospheric dispersion and injects the YJH light into the fiber link. The visible light goes straight into the HARPS “bonnette”
2. The *fiber link* which includes several provisions to scramble the light in addition to it obvious function of guiding the light from the telescope to the spectrograph. The purpose of the light scrambling is to stabilize the position of the photocenter of the light to a tiny fraction of the fiber diameter since a shift if the photocenter is interpreted as a radial velocity once the light is dispersed in the spectrograph.
3. The *spectrograph* itself

It was decided early in the conceptual design phase that NIRPS would be Adaptive Optics assisted to minimize its cost, minimize it dimensions and maximize it stability.

3. FRONT-END DESIGN

3.1 Optical set-up

One of the original points of the NIRPS is that it is assisted by an Adaptive Optics (AO) system. The common path is made of a dichroic filter a fold mirror, an atmospheric dispersion corrector a collimator and a 241 actuator deformable mirror. The differential tip-tilt between the HARPS beam and the NIRPS beam is taken care by a custom high stiffness high precision mount on which the deformable mirror is mounted. After a dichroic extracting the light to the wavefront sensor a simple doublet focuses the science light onto the fiber heads which perform the F-ratio adaptation. On the focal plane of the fiber heads, a pieced mirror reflect the halo to a viewing camera. This camera serves two purposes: using a high magnification lens it allows a detailed look at the PSF produced by the AO and the characterization of the Non-Common Path Aberrations (NCPA). Using a smaller magnification lens looking at the distribution of the halo around the hole in the pierced mirror it serves for the fine guiding of the science beam to optimize coupling and uniformity.

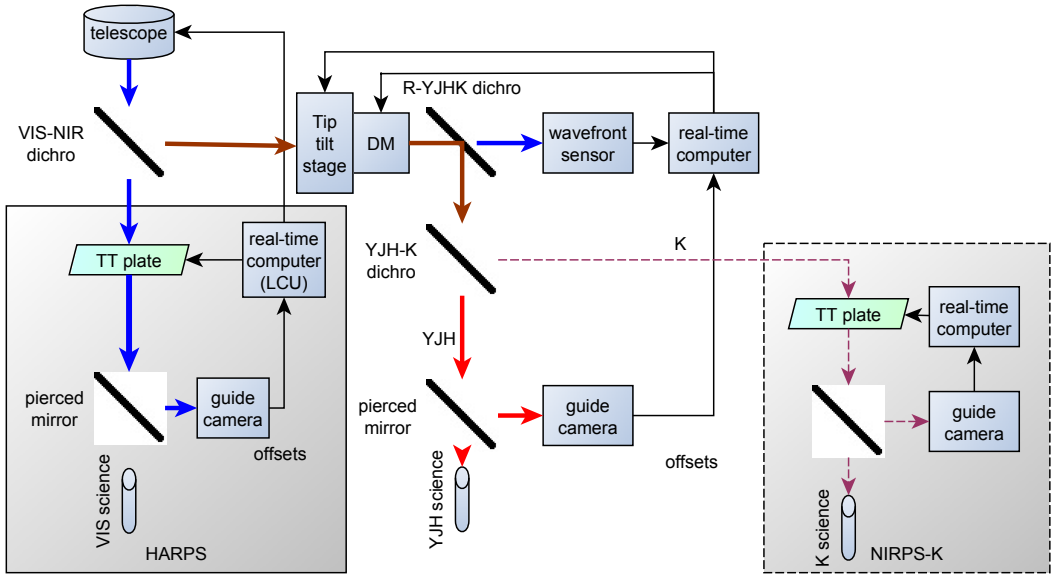

Figure 2 - Functional diagram of the NIRPS front end.

4.2 Adaptive optics fiber injection module

The main goal of the adaptive optics (AO) module is to break the conservation of the telescope “étendue”, which mainly drives the size of the high resolution spectrographs. The AO system will allow to inject the light into fibers twice as small as those needed for a classical seeing-limited spectrograph without losing in collecting efficiency and thus having a very compact spectrograph design. The top level requirement regarding the AO performances is to couple 50% of the light into fibers as small as possible using a guide star magnitude as faint as I=12 under median seeing conditions at La Silla.. This is equivalent of what HARPS couples in 0.9” without fiber optics.

The star magnitude (I=12) is derived from the expected candidates coming from the TESS survey (focused on the 150 brightest M-type stars)[2]. And the median seeing at La Silla is 0.9”.

To meet this requirement, we derived the optimal size of the fiber and AO configuration[3]. We found an ideal size of fiber of 0.4” (diameter projected on the sky) for an AO system using a 14x14 Shack-Hartmann wavefront sensor (WFS) and a 15x15 deformable mirror (DM). The system will run between 250 and 1000 Hz depending on the guide star magnitude. We can notice here than the AO system will work “on-axis”, i.e. the guide star is the scientific target.

The WFS will operate in the 700-950 nm range, which is the gap between the wavelength range of HARPS and NIRPS and thus allow us to operate simultaneously the both instruments. For the WFS camera, we opted for an OCAM^{2}K (EMCCD) with a custom lenslet array (16x16 subapertures with only 14x14 used for the sensing). The lenslet gives us 15x15 pixels per subaperture and allows us to track the telescope and DM missregistration by monitoring flux levels on

the outer ring of subapertures. The advantages of such a camera are mainly the low read-out noise (<0.3e$^-$) and the very high quantum efficiency especially in our range of interest which allow us to gain up to 0.5 magnitude on the guide stars compared to other cameras.

The DM required 15x15 actuators, we therefore opted for an ALPAO DM241 (with the high speed option). The advantages of such a DM are the large stroke (tip-tilt stroke ≈ 50 µm Peak to Valley), linearity (0.03%) and fast settling time (0.44 ms). Due to the HARPS+NIRPS simultaneous observation mode, a differential tip-tilt between the two beams (visible and near infra-red) before the injection into fibers is expected. The DM will be therefore mounted on a tip-tilt stage (with ±0.5° amplitude, i.e. ± 40" on the sky) to compensate this differential tip-tilt and let us enough stroke on the DM to compensate the atmospheric tip-tilt and higher order turbulences.

Regarding the real time controller of the AO, we also opted for an off-the-shelf product made by ALPAO: ACE. It consists in a Matlab© Toolbox where all the hardware (WFS + DM) is interfaced in. ACE (the fast version using a dedicated server) can reach a latency of 83 µs.

In order to test our hardware before the integration of the instrument, we designed a test bench including a phase screen to simulate the atmospheric turbulences. The bench allows us to characterize the AO performance under different conditions such as the star magnitude and the seeing and validate the coupling of an AO-corrected PSF into the NIRPS fibers.

Table 1. Expected performances of the AO system. The encircled energy (EE) over the NIRPS wavelength range (1.0-1.8 µm) for different seeing conditions and guide star magnitudes is showed.

	Seeing (λ = 0.5 µm)		
Star magnitude	**0.7" (25% best cases)**	**0.9" (50% best cases)**	**1.2" (75% best cases)**
I=10	73±1%	66±1%	54±2%
I=12	63±1%	53±2%	39±2%
I=13	50±2%	38±2%	23±1%

3.2 Fiber coupling

NIRPS High Accuracy fiber only contains 10 to 35 modes and thus works in the so-called few-mode regime. In this regime, geometrical optics does not apply anymore: we must compute the coupling ρ_{lm} as the overlap integral between every individual mode E_{lm} and the instantaneous electric field in the telescope pupil E_{tel} (which includes the corrected wavefront error), so that:

$$\rho_{lm} = \frac{|\iint E_{tel} E_{lm}^{*} dA|^2}{\iint |E_{tel}|^2 dA \cdot \iint |E_{lm}|^2 dA}$$

The total coupling in the fiber in then obtained as $\rho = \Sigma \rho_{lm}$. Using wavefront residuals from our AO simulations, we show in Figure 3 that coupling efficiency is equivalent to Encircled Energy (EE) for $N_{mode} \geq 15$ ($\lambda < 1.5$µm for NIRPS). For $\lambda > 1.5$µm, we observe that $\rho >$ EE: in this condition, the modes are also guided through the fiber cladding and are therefore able to couple speckles that fall within a 0.5-0.6" diameter area.

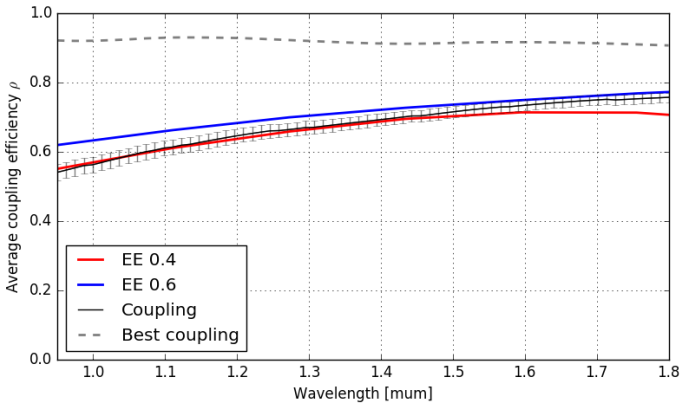

Figure 3 - NIRPS expected fiber coupling (black) compared to EE in 0.4" and 0.6" for a bright star and median seeing. Dotted line shows the maximum expected coupling without turbulences.

3.3 Opto-mechanics and alignment

The front end is directly attached at the back of the ESO 3.6m telescope rotator. The existing HARPS bonnette is kept as is and its position wrt to the telescope remains the same. However the bracket on which it is mounted, is completely new. Indeed, the new structure supports both the HARPS bonnette and NIRPS front-end optics.

The NIRPS front-end consists of:

- NIRPS Cassegrain adapter: This part is mounted on the 3.6 telescope rotator interface. Moreover, it serves as the optical bench on which most of the NIRPS optical components are mounted.
- HARPS Front-end bracket : it interfaces to the existing HARPS bonnette, hold the the VIS-NIR dichro, the HARPS guiding camera
- 3 monopods that are holding the HARPS Front-end bracket. They are mounted onto the NIRPS Cassegrain adapter.

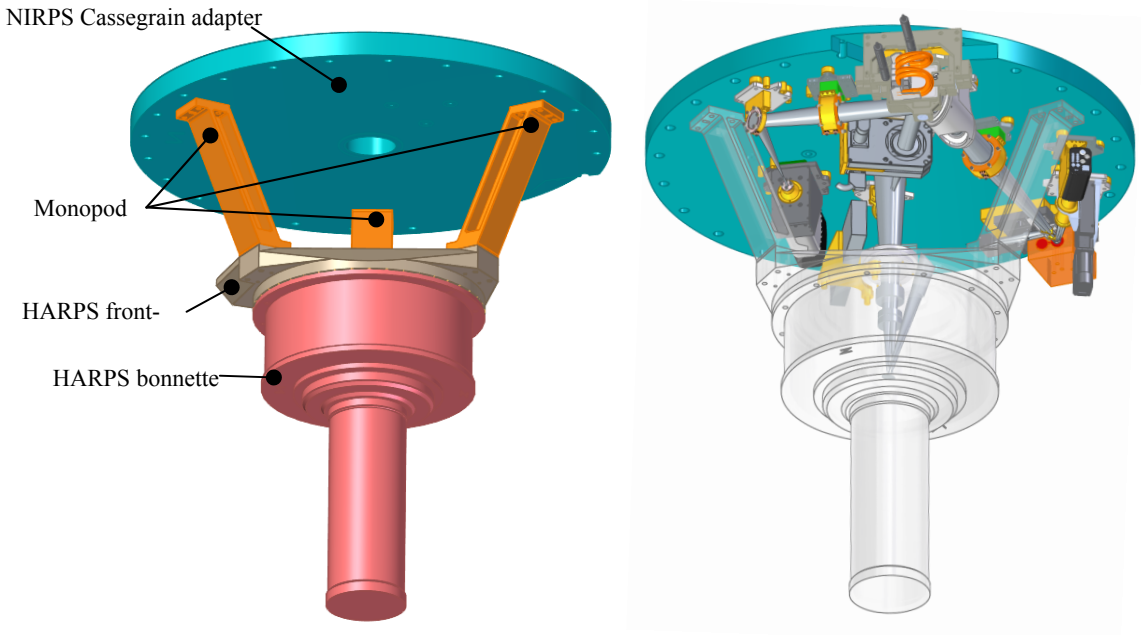

Figure 4 - Location of the different components of the support structure, optical components, mechanisms and cameras.

The front-end optical components, cameras and mechanisms are held by mounts or brackets. All these subassemblies are attached to the front-end support structure with the same interface plate. A dedicated positioning jig has been developed to support the alignment of these subassemblies. It is made of micro-adjustment screws and Linear Variable Differential Transformer (LVDT) gage probes. It allows the adjustment of 5 DoFs (tilt, tip and the 3 translations x,y and z) and will be used for the alignment of all subassemblies. During the alignment procedure of a subassembly, its current position is measured by a portable Coordinate Measurement Machine. Based on the position of the optical component of the subassembly given by the optical design, a software computes the required rotations and translations needed to reach the nominal position. The operation is repeated until the residual errors are acceptable. The subassemblies are then shimmed and lateral end-stops are positioned to constrain the motion of the subassembly and allows an accurate re-positioning of the subassembly after dismounting. A prototype has been built to the test the performances of the alignment procedure. First results show positioning accuracy <10µm and re-positioning accuracy ≅20µm , a factor 2.5 to 5 better than the alignment tolerances of our design.

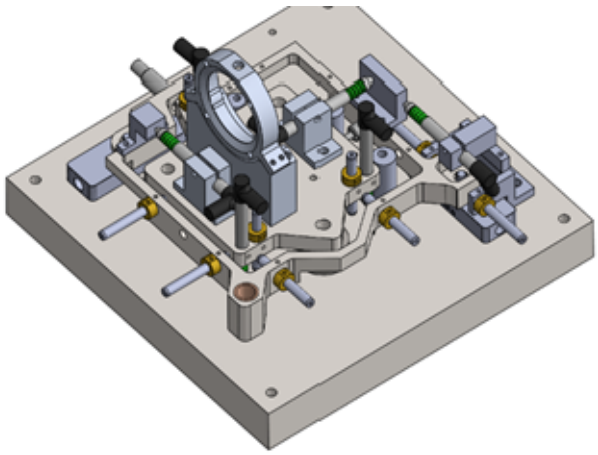

Figure 5 - Prototype built for the testing of mechanical alignment.

4. PSF STABILITY, SCRAMBLING

Modal noise is the instability in the fiber output illumination leading to instability of the spectrograph Line Spread Function (LSF), i.e. to RV noise. Any disturbances at the fiber entrance like guiding errors or along it (e.g. varying bend stress) can be transported up to the fiber output, hence generating a change of the spectrograph LSF. Losing this information to get a perfectly stabilized LSF is called scrambling.

Modal noise originates from the combination of two effects if the effect:

1. An incomplete filling of the fiber near- and/or far-field;
2. Intermodal phase variations, corresponding in geometric optics to the difference of optical path travelled by rays with different arrival angles.

The combination of those effects generates at the fiber output a speckle pattern that contains to some degree information on the injection conditions and local environment. Those effects in addition slowly evolve with wavelength, requiring bandpass of several 10nm to average.

NIRPS is an instrument particularly sensitive to modal noise since its fibers work in the so-called *few-mode* regime, with only 10-35 modes guided. Since modal noise is proportional to λ/a (a being the fiber core size[4] , it is 5 to 10 times higher than in a seeing-limited, visible instrument like HARPS. In these conditions, it may limit RV precision to 5-10 m/s, even with well proven scrambling solutions, namely:

1. **Double scramblers** that exchange near- and far-field;
2. **Octagonal/rectangular fibers**.

To achieve the goal of 1 $m.s^{-1}$ RV precision, two additional scrambling solution have been studied:

3. **Adaptive Optics** – We will make use of the many degrees of freedom of the AO system to actively scramble modes at the fiber input. At this stage, a simple tip-tilt scan has proven to be the most efficient - and terms like defocus to be worsts- both in terms of scrambling and coupling efficiency. Mode selective coupling is actually possible by injecting specific DM shapes, but it quickly costs photons[5]. This could be acceptable for brightest targets though.
4. **Fiber Stretcher** – In order to stabilize the LSF for any modal content, we also use a fiber stretcher that actively modulates the phase between the modes (Figure 6): the result is an azimuthally symmetrized LSF, whatever the modal content (i.e. whatever the injection conditions). This device shall be able to beat slowly evolving effects like temperature drifts, telescope pointing and observation-to-observation variations (e.g. different H.A for a same target). The fiber stretcher demonstrated scrambling gain equivalent to the double scrambler, with a transmission of ~90% that did not degrade after more than 6 months of constant operation.

The combination of those 4 devices have demonstrated their scrambling efficiency in the lab, and let us conclude that 1 $m.s^{-1}$ RV precision shall be achieved with NIRPS[3].

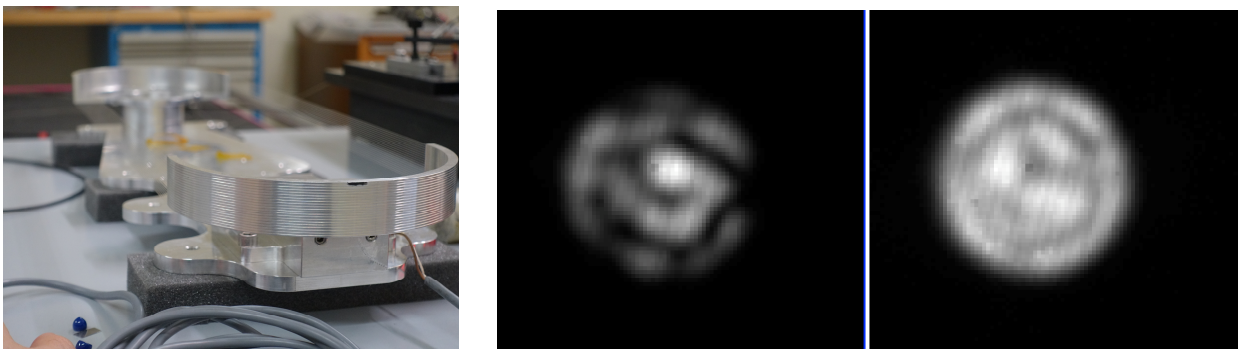

Figure 6 – *Left*: Picture of the fiber stretcher prototype, offering 8mm optical stretch up to 20 Hz. *Middle*: output of a fiber in the stretcher (turned OFF) with a laser source λ=980nm. *Right*: same as Middle, with stretcher ON.

5. SPECTROGRAPH DESIGN

5.1 Optical design

The NIRPS spectrograph includes one parabola working in triple pass, a R4 echelle grating (90 mm x 320 mm with a blaze angle of 76 degrees and ~ 13.3 gr/mm), a flat folding mirror, an optical train of 5 cross disperser ZnSe prisms, a refractive camera, and a detector. The optical path sequence is the following:

- The fiber end tip is converted to the spectrograph input object (29 um core fiber @ F4.2 to 55um @ F8.0)
- The parabola collimates the fiber beam (1st pass on the parabola) and sends it to the grating.
- The grating diffracts the collimated beam and sends it back to the parabola.
- The parabola focuses the diffracted collimated beam close to the input object point (2nd pass on the parabola).
- The flat mirror located in the intermediate image plane folds the diffracted focused beam back to the parabola.
- The parabola collimates the diffracted focused beam (3rd pass on the parabola).
- The diffracted collimated beam then passes through the 5 refractive prisms separating the grating orders.
- The refractive camera focuses the diffracted collimated beam on the detector.

The optical design of the refractive camera is seriously constrained due to the limited range of optical materials with known indices of refraction and coefficients of thermal expansion (CTEs) at cryogenic temperatures within the spectral range of the instrument. Glasses are mostly limited to calcium and barium fluoride (CaF2, BaF2), zinc sulfide and selenide (ZnS, ZnSe), Cleartran™, fused silica, and S-FTM16. All the optics being kept within the cryostat at 80K, the optical design is prepared using a custom catalogue of refractive indices of materials at 80K (available from data in [6], [7] and [8]). This in order to obtain a complete as built "cold" optical prescription of the instrument. The optical elements thicknesses and radiuses are then manually calculated by using the proper CTE from 80 to 270K for each individual

component. The air space (vacuum) between the elements is also calculated according to the mechanical material CTEs. We thus obtain a "hot" prescription of the design. This will be the version we get in the laboratory when mounting all the components. Both the cold and hot version of the design are then transferred to the mechanical designer for him to double-check and prepare the final mechanical design.

The final design of the camera is composed of 4 lenses, one CaF2, one S-FTM16, and two ZnSe elements. The first three lenses are spherical elements and the fourth lens has a cylindrical surface. In order to minimize the number of optical elements, the design depends on position and angle offsets (relative to the first two lenses) of the two ZnSe lenses that are in front of the detector. Alignment will be difficult due to the presence of fold mirrors (parabola, grating and flat) because the optical system does not share a common optical axis. It is proposed that the branches of the folded system be aligned by making the mirrors and lens housings adjustable in orientation.

Figure 7 shows the order distribution on the detector. The first order in the blue region (bottom of figure) covers the wavelength range from 973.79 nm to 980.35 nm while the top one in red covers the range from 1786.33 nm to 1802.91 nm. The distance between the orders varies from 38.9 pixels in the red up to 78 pixels in the blue portion of the spectral range. The encircled energy is > 80% in 3 pixels at all wavelengths and this value is maintained for a detector range of displacement of +/- 200 µm from its nominal position. Figure 8 shows the resulting spectral resolution as a function of wavelength computed using the compressed image profiles of a 29-um F/4.2 core diameter fiber along a direction perpendicular to the dispersion.

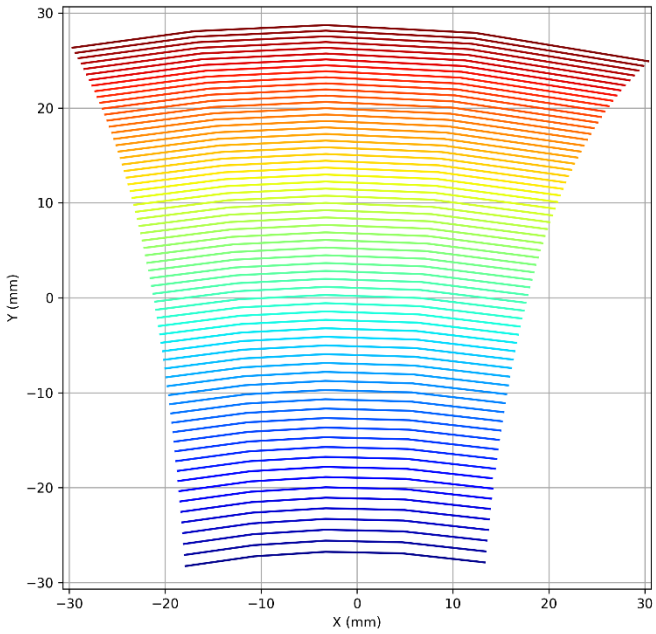

Figure 7 – Order distribution on the detector. The first order in the blue region (bottom of figure) covers the wavelength range from 973.79 nm to 980.35 nm while the top one in red covers the range from 1786.33 nm to 1802.91 nm.

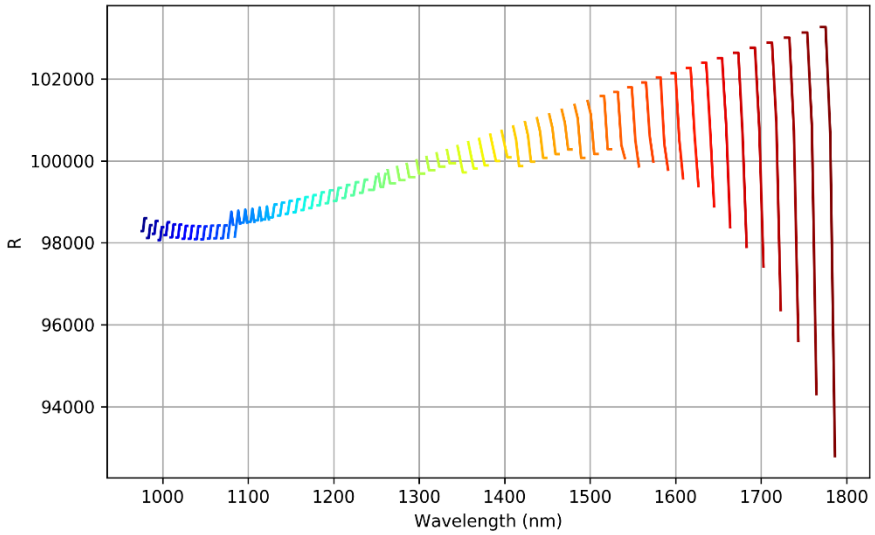

Figure 8 – NIRPS expected spectral resolution as a function of wavelength obtain from the optical design.

The optical design of the refractive camera contains a lens that is rather close to the detector (~ 10 mm) A ghost analysis was performed using a Zemax non-sequential ray tracing version of the design to identify possible ghosting issues. The analysis show that the ghosts produced are, at all wavelengths within the spectral range, about six orders of magnitudes below the signal of interest. The analysis also indicates that the most important sources of ghosts are the last two lenses of the camera. At all wavelengths examined, the signal is within a patch of about 60 pixels in diameter and mostly caused by the lens surface that is the closest to the detector.

5.2 Cryostat and opto-mechanics

The optical system of the spectrograph is cryogenic, with operating temperature of 80K. It resides in a cylindrical vacuum vessel of 1120 mm outside diameter, and 3366 mm long in operational mode (when closed). The cylindrical portion of the cryostat slides along its axis to allow easy access to the optical housing (see Figure 9).

The optical housing (optical bench) is located in a horizontal position. It is supported at two points from a cold support frame by a hexapod type arrangement (Figure 10). Cold support frame combines active cold shield and structural support.

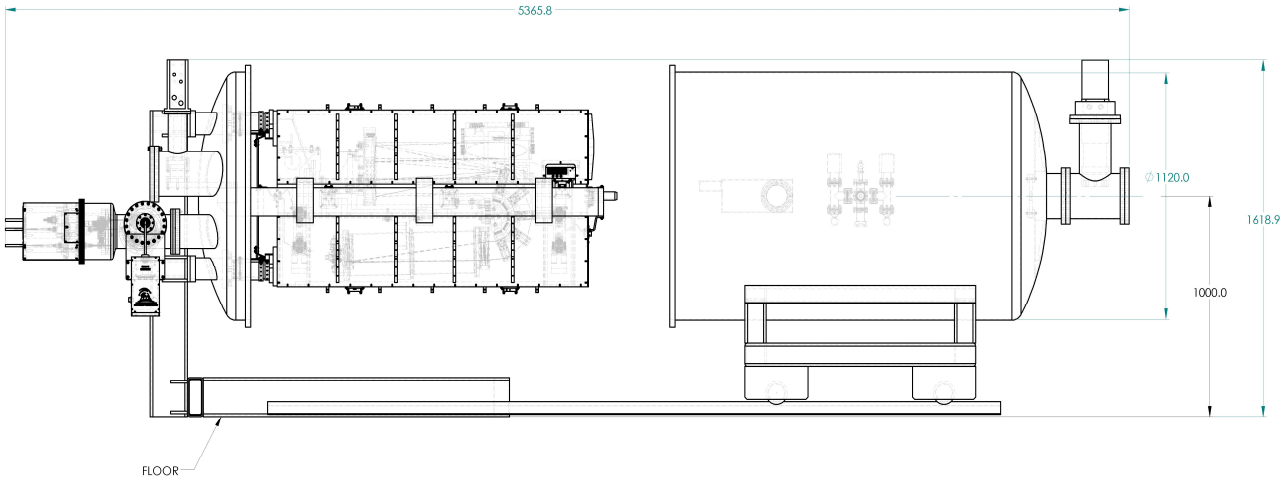

Figure 9. Open cryostat, side view.

The hexapod supports are made from G10 to insulate the optical bench from the cold active shield/cold support frame. The cold internal support frame/active shield is cantilevered from the stationary end of the cryostat. It rests on four G10 flexures on the fixed end. For the ease of maintenance all instrument feedthroughs and cryo-coolers are located on the stationary parts of the cryostat.

Generally speaking, symmetrical systems are inherently more stable. Thus, one of the fundamental design intents in the development of the mechanical concept of the cryostat was to keep system symmetrical around long vertical plane.

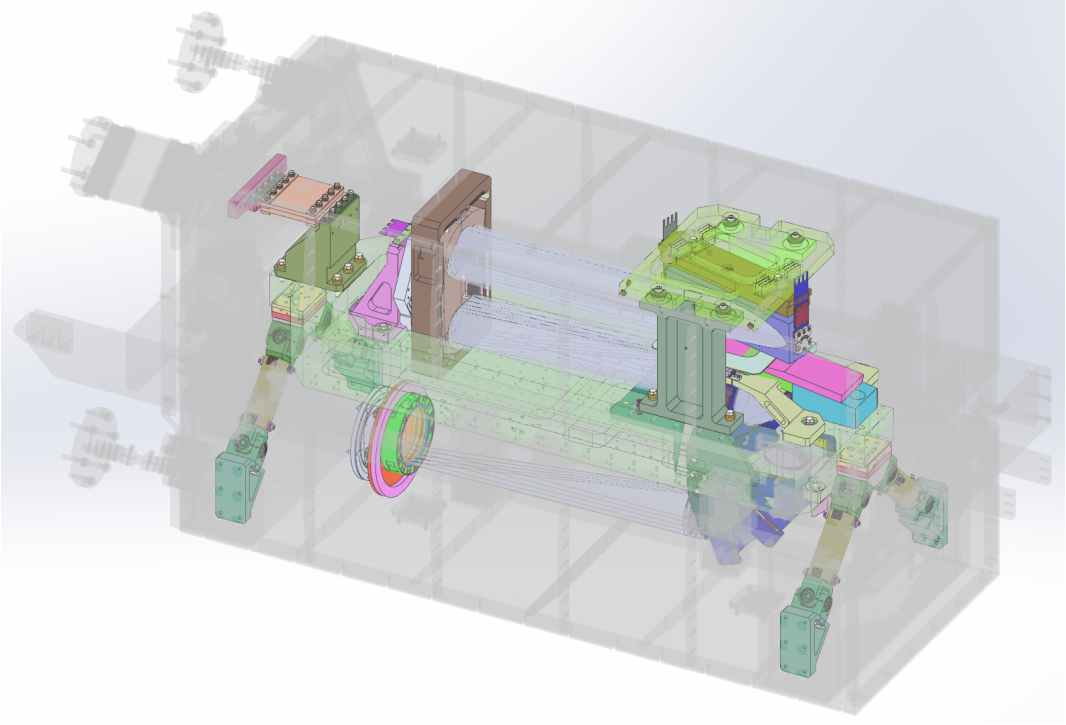

Figure 10. The optical system within the active cold shield enclosure.

Thermal control for the NIRPS spectrograph is a very close adaptation of the thermal control utilized for the SPIRou instrument. It was demonstrated in a test, that thermal stability of the SPIRou optical bench to be better than 1 mK. This level of thermal stability was adopted as a requirement for the NIRPS project. General approach to achieving temperature stability is to keep conductive connections between the system and the environment to a minimum, and to actively stabilize temperature in the areas conductively and radiatively coupled to the environment, as well as in the areas of internal heat dissipation (detector).

In total, inside the vacuum vessel, we are going to have 18 points with active thermal control loops.

High precision thermal control (< 1 mK) will be used for all critical points conductively coupled to the optical system/optical housing (five in total). Which are: two optical bench supports, cable feed-thru assembly, and also two locations in the detector package. The measuring device for the precision thermal control is MicroK thermometry bridge and multiplexer manufactured by Isotech.

The temperature in the rest of the thermal control loops is measured using 12 channel Lakeshore 224 thermal monitors. Combination of Lakeshore 224 and Cernox LSCX-1080-AA four wire sensors is capable of ±9 mK short term precision (as per manufacturers specifications).

The optical housing is surrounded by an active shield covered with MLI blankets on the inside and outside. The active shield is also kept at the operating temperature of 80K, but its temperature stability can be controlled to a more relaxed

range of ± 9 mK (stability of the Lakeshore 224), due to the fact that radiative thermal coupling is relatively weak, when compared to thermal conduction through the supports.

In both cases, for high and low precision control points, we will use industry standard PLC systems to drive heaters in a closed loop with temperature readings from MicroK and Lakeshore as inputs. Massive cold bus (Figure 11) made from copper plate will be used to lift heat from the thermal control points throughout the system.

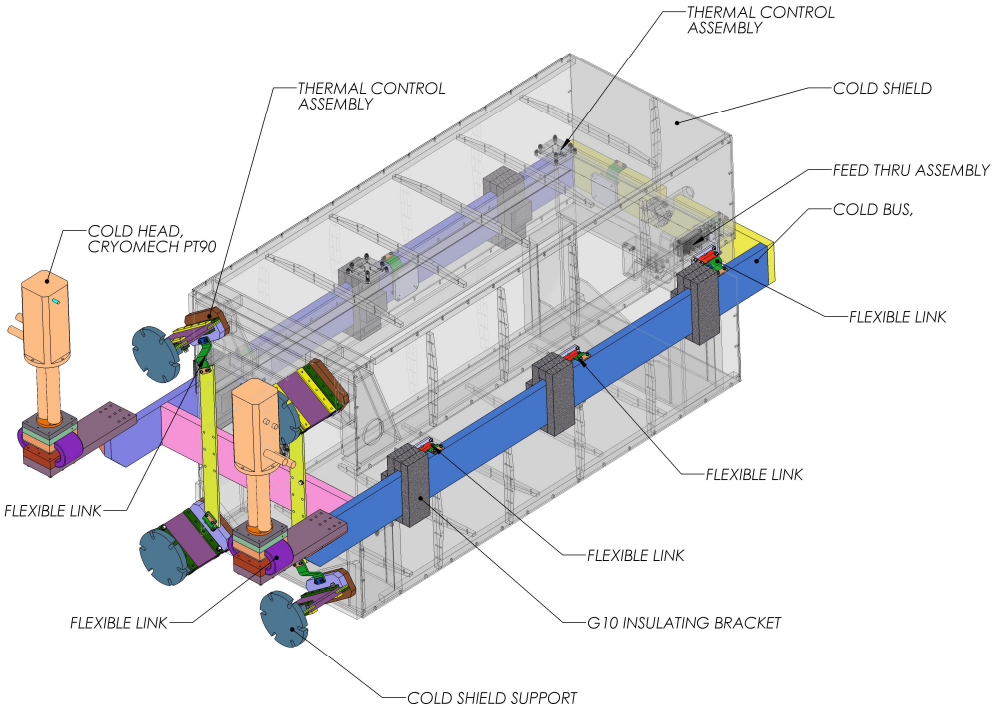

Figure 11. Main elements of the thermal network (optical system is not shown).

Optical elements will be mounted utilizing glued flat flexure supports. The parabola mirror optical mount on Figure 12 is a good example. It shares the same basic features with the other cryogenic optical mounts in the instrument: it is symmetric around vertical plane, and the optical element is suspended on flat flexures. Flexures are glued to the elements, and are made from the material with cumulative thermal expansion matched close to the substrate of the optical element.

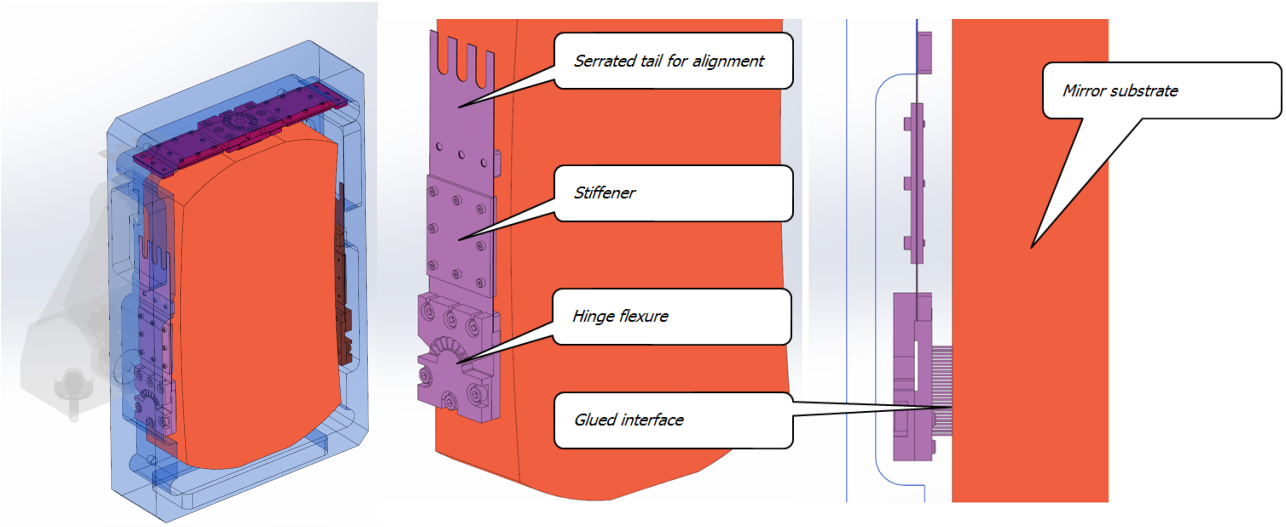

Figure 12. Parabola optical mount.

6. PERFORMANCE BUDGET

One of the primary goals of NIRPS is the detection and characterization of Earth-like planets in the habitable zone of low-mass stars and it must be able to achieve a radial velocity precision of 1 m/s to reach this goal and be competitive against other similar instrument being developed elsewhere. The error budget of NIRPS is strongly inspired from the experience of HARPS and SOPHIE at the 1.93-m OHP telescope (respectively 0.6 and 2 m/s of precision achieved). We have performed a detailed analysis of the RV error budget of NIRPS which is summarized below. This includes the photon noise from the target itself, the finite accuracy of the exposure mid-point, the wavelength solution, the intrapixel response, the injection stability and, most importantly, modal noise.

The fundamental limitation to RV measurements is due to **photon noise** and has been described by Bouchy et a in l[9]. A detailed analysis of the *Q* factor for Barnard Star (the only M dwarf with an *observed* spectrum in the *JHK* bands at R~100 000) is given in [10]. Barnard Star is representative of mid-Ms that will be observed with NIRPS, and an accuracy of 2.5 m/s for an SNR =100 in *J*, or correspondingly, an RV precision *from photon noise alone* of 1 m/s for an SNR = 250. We do *not* include this contribution in the instrument RV budget, as this will be target-dependent and cannot be improved upon by better instrumentation. The spectrograph's error budget is therefore considered to be the budget for all sources *other than photon noise from the stellar spectra*.

RV measurement at the m/s accuracy requires knowledge of the flux-weighted **midpoint of the exposure** down to a few seconds, significantly shorter than the ~5 minute exposures for typical targets. To obtain the mid-exposure time we will take advantage of the non-destructive readout capabilities of the NIRPS science array to obtain measurements on the incident flux on a timescale of 5.5s and to monitor the variation of flux during the exposure. Mid-exposure times will be computed by the detector control computer from the individual readouts of the science array. Barycentric velocity changes have two causes, the Earth's rotation at the observer's latitude and the Earth's orbital motion. Barycentric velocity correction is depends on the target position on the sky, and in the worst-case for a star on the ecliptic can vary at most of 10 cm/s in a delay of 3 s. We conservatively allocate 0.10m/s to this item in our error budget.

Wavelength solution will be performed using a mixed approach combining hollow-cathode lamp (HCL) and stabilized Fabry-Perrot (FP). While only the HCL provides a physical anchoring of the wavelength solution, the fact that the FP peak position can be traced to simple physics and can be used to significantly reduce errors in the solution. The main limitation here will arise from the finite SNR reachable within a calibration exposure. Assuming the same photon noise as in Bauer 2015, we will predict a ~8 cm/s contribution to the error budget from the calibration files, with a very small systematic component. We set an upper limit of 0.1 m/s on this contribution to the error budget.

Numerical simulations including realistic **intrapixel response** for infrared arrays[11] were performed to assess the impact on RV measurements. The impact on the RV measurement will be a very small increase in the noise due to the imperfect flat-fielding due to the difference of structure between the stellar and flat-field intra-pixel illumination. We set an upper limit in our RMS budget of **<10 cm/s** for this term and note that the true value is expected to be much smaller as this is only for a single diffraction order and these are expected to average-out incoherently over the ~50 useful orders within NIRPS bandpass.

The NIRPS spectrograph is installed in an evacuated and temperature-controlled vacuum enclosure ($<10^{-5}$ mbar and 1 mK stability). This minimizes, to a very large extend, RV drifts produced by temperature, air pressure and humidity change. With a similar concept ($< 10^{-2}$ mbar and 5mK stability) HARPS provide a drift lower than 1m/s in one day. The goal is to obtain similar **stability of 0.50 m/s in a night** and **drift between calibration and science fibers <0.1m/s** during the same time span.

Any variability in the light **injection in the spectrograph** from the fiber and the slicer will introduce an RV variation by shifting the image position in the detector, and as such contribute to the error budget. For a fiber design without double scrambler, the centering of the stars at the entrance of the fiber has important consequences on the light distribution at the fiber output. This directly translates into the spectrum on the detector and therefore into spurious RV variations[1]. The use of an octagonal fiber on the fiber link of NIRPS strongly increases the scrambling power of the fiber and limit this effect. Experience from SOPHIE[12] suggest a scrambling of a factor 700-2000. The AO system guiding stability projected onto the science array corresponds to a very small contributor to the stability of the instrument, at the **0.05 m/s** level**.**

NIRPS is particularly sensitive **to modal noise** because it operates in the near infrared and it uses an AO to divide by 2 the fiber size. Hence the number of guided modes in NIRPS High Accuracy fiber is between 15 and 30 (~30 times less

than HARPS. As mentioned in section 5 a significant effort is ongoing to understand and reduce modal noise and allow measurements at the required level of 1m/s. Several modal noise mitigation devices will be implemented. The fiber train will pass through a **double scrambler** that has demonstrated improvement in near-field stability of a factor of 2 to 5. A **fiber stretcher** (similar to a fiber delay line) will be used to change the phase between all the modes and to homogenize the near- and far-field illumination for any given modal configuration. This device has a minimal impact on the modal distribution itself, conversely to fiber shaking devices. The scrambling of modes will be the function of the AO system and double scrambler. The amplitude of phase modulation is also much higher with the stretcher than by shaking. The AO system will be used to scramble the fiber modes by dynamically injecting known Zernike aberrations. Computations show that tip and tilt are the most efficient modulations that the AO system can produce to scramble the fiber mode modes with the least impact on coupling efficiency. Detailed simulations of the cumulative effect of these mitigation strategies predict an RV impact of <50 cm/s for the modal noise averaged over then entire NIRPS domain for the High Accuracy Fiber.

Table 2. Global RV budget breakdown.

RV error	**Contribution to budget**
Wavelength calibration	0.10 m/s
Spectrograph stability	0.50 m/s (0.10 with simultaneous calib)
Guiding	0.05 m/s
Modal noise	0.50 m/s
Mid-point of exposure	0.10 m/s
Intrapixel response	0.10 m/s
Total	**0.73 m/s**

7. CONCLUSION

The design of NIRPS is meets the top level requirements. It is careful mix of well-known solutions inherited from previous projects, of standard industrial solutions, in particular for the control system and cutting edge innovative solution to carry this instrument beyond today's state-of-the-art, like adaptive optics feed and scrambling. This combination allows a very fast development cycle, with a kick.off in Jan 2016 and a commissioning planned for the end of 2019.

The combination of HARPS in the visible and NIRPS in the 950-1800nm band with 100'000 resolution holds great promises in the detection of small planets in the HZ of M stars with both the sensitivity at the $1ms^{-1}$ mark and the ability to discriminate activity form RV by chromatic alalysis.

ACKNOWLEDGEMENTS

The Swiss share of this work has been carried out within the framework of the National Centre for Competence in Research PlanetS supported by the Swiss National Science Foundation. The authors acknowledge the financial support of the SNSF.

REFERENCES

[1] Lovis C. et al. The exoplanet hunter HARPS: unequalled accuracy and perspectives toward 1 cm s^{-1} precision, SPIE 6269-25, 2006
[2] Sullivan, P. W. et al, 2015, ApJ, 809, 77
[3] Conod U. et al. 2016, Proc. SPIE, 9909, 41
[4] Baudrand, J., & Walker, G. A. H. 2001, PASP, 113, 851
[5] Blind N. et al., 2017, *proc. of AO4ELT5* (in prep.).

[6] W. J. Tropf, Temperature-dependent refractive index models for BaF2, CaF2, MgF2, SrF2, LiF, NaF, KCl, ZnS, and ZnSe, Opt. Eng. 34, no. 5, pp. 1369-1373, 1995. doi:10.1117/12.201666
[7] W. R. Brown, H. W. Epps, D. G. Fabricant, The cryogenic refractive indices of S-FTM16, a unique optical glass for near-infrared instrument, Publ. Astron. Soc. Pac. 116, pp. 833-841, 2004
[8] D. B. Leviton, B. J. Frey, T. J. Madison, Temperature-dependent refractive index of CaF2 and Infrasil 301, Proc. SPIE 6692, pp. 669204, 2007. doi:10.1117/12.735594
[9] Bouchy F. et al., 2001, A&A 374, 733
[10] Artigau et al[5]. 2017, AJ, submitted
[11] T. Hardy; Chris Willot; J. Pazder, Intra-pixel response of the new JWST infrared detector arrays. SPIE 9154, 2014
[12] Boisse et al. 2011, arXiv1001:0794